The Astrophysical Journal Supplement Series, 246:31 (10pp), 2020 February https://doi.org/10.3847/1538-4365/ab53d2

Clustering of Intermittent Magnetic and Flow Structures near *Parker Solar Probe*'s First Perihelion—A Partial-variance-of-increments Analysis

Rohit Chhiber[1,2], M L. Goldstein[3,4], B. A. Maruca[1,5], A. Chasapis[1,6], W. H. Matthaeus[1,5], D. Ruffolo[7], R. Bandyopadhyay[1], T. N. Parashar[1], R. Qudsi[1], T. Dudok de Wit[8], S. D. Bale[9,10,11], J. W. Bonnell[9], K. Goetz[12], P. R. Harvey[9], R. J. MacDowall[13], D. Malaspina[6], M. Pulupa[9], J. C. Kasper[14,15], K. E. Korreck[15], A. W. Case[15], M. Stevens[15], P. Whittlesey[9], D. Larson[9], R. Livi[9], M. Velli[16], and N. Raouafi[17]
[1] Department of Physics and Astronomy, University of Delaware, Newark, DE, USA; rohit.chhiber@nasa.gov
[2] Code 671, NASA Goddard Space Flight Center, Greenbelt, MD, USA
[3] Code 672, NASA Goddard Space Flight Center, Greenbelt, MD, USA
[4] University of Maryland Baltimore County, Baltimore, MD, USA
[5] Bartol Research Institute, University of Delaware, Newark, DE 19716, USA
[6] Laboratory for Atmospheric and Space Physics, University of Colorado, Boulder, CO, USA
[7] Department of Physics, Faculty of Science, Mahidol University, Bangkok, Thailand
[8] LPC2E, CNRS and University of Orléans, Orléans, France
[9] Space Sciences Laboratory, University of California, Berkeley, CA, USA
[10] Physics Department, University of California, Berkeley, CA, USA
[11] The Blackett Laboratory, Imperial College London, London, UK
[12] School of Physics and Astronomy, University of Minnesota, Minneapolis, MN, USA
[13] Code 695, NASA Goddard Space Flight Center, Greenbelt, MD, USA
[14] Climate and Space Sciences and Engineering, University of Michigan, Ann Arbor, MI, USA
[15] Smithsonian Astrophysical Observatory, Cambridge, MA, USA
[16] Department of Earth, Planetary, and Space Sciences, University of California, Los Angeles, CA, USA
[17] Johns Hopkins University Applied Physics Laboratory, Laurel, MD, USA
Received 2019 September 16; revised 2019 October 28; accepted 2019 October 31; published 2020 February 3

Abstract

During the *Parker Solar Probe*'s (*PSP*) first perihelion pass, the spacecraft reached within a heliocentric distance of $\sim 37\ R_{\odot}$ and observed numerous magnetic and flow structures characterized by sharp gradients. To better understand these intermittent structures in the young solar wind, an important property to examine is their degree of correlation in time and space. To this end, we use the well-tested partial variance of increments (PVI) technique to identify intermittent events in FIELDS and SWEAP observations of magnetic and proton-velocity fields (respectively) during *PSP*'s first solar encounter, when the spacecraft was within 0.25 au from the Sun. We then examine distributions of waiting times (WT) between events with varying separation and PVI thresholds. We find power-law distributions for WT shorter than a characteristic scale comparable to the correlation time of the fluctuations, suggesting a high degree of correlation that may originate in a clustering process. WT longer than this characteristic time are better described by an exponential, suggesting a random memory-less Poisson process at play. These findings are consistent with near-Earth observations of solar wind turbulence. The present study complements the one by Dudok de Wit et al., which focuses on WT between observed "switchbacks" in the radial magnetic field.

Unified Astronomy Thesaurus concepts: Interplanetary turbulence (830); Solar wind (1534); Interplanetary discontinuities (820); Solar corona (1483); Magnetohydrodynamics (1964)

1. Introduction

Turbulence has diverse effects in fluids, magnetofluids, and plasmas such as the interplanetary medium and the solar wind (Pope 2000; Biskamp 2003; Matthaeus & Velli 2011). While far less is understood about the latter case compared to the two fluid cases, plasma turbulence apparently shares with classical turbulence its capacity to greatly enhance transport. This includes the transport of energy across scales, suggested by the presence of characteristic second-order statistics such as wavenumber spectra (Bruno & Carbone 2013), as well as third-order statistics (Politano & Pouquet 1998) which quantitatively (and in some cases, approximately; see Hellinger et al. 2018) characterize the rate of cascade across scales. Turbulence also produces intermittency (Sreenivasan & Antonia 1997; Matthaeus et al. 2015), and the associated coherent structures, including current sheets and vortices (Zhdankin et al. 2012; Parashar & Matthaeus 2016), are responsible for spatial concentration of physical processes observed in heliospheric plasmas, such as heating, heat conduction, temperature anisotropies, and local particle energization (Osman et al. 2011; Greco et al. 2012; Karimabadi et al. 2013; Tessein et al. 2013). Coherent current and field structures can also significantly influence the transport of field lines and charged particles, affecting distributed transport and acceleration (Ruffolo et al. 2003; Zank et al. 2014; Tooprakai et al. 2016). There are, therefore, numerous applications that provide motivation for better understanding of the occurrence rate and distribution of intensities of coherent structures such as current sheets.

Traditionally, sharp changes in the magnetic field have been classified as various types of "discontinuities," which are convected or propagated as approximate solutions of linear ideal magnetohydrodynamics (MHD; Burlaga & Ness 1969; Tsurutani & Smith 1979; Neugebauer et al. 1984; Neugebauer & Giacalone 2010). The ongoing recognition that these structures are generated rapidly and generically by turbulence changes the nature of their study at a level of basic physics. As

a consequence of turbulence, coherent structures are a manifestation of nonlinear dynamics and intermittency, a direct reflection of the higher-order correlations that are implied by the cascade process itself (Oboukhov 1962; Frisch 1995). Such higher-order statistical correlations are routinely observed in space observations in plasmas such as the solar wind (e.g., Horbury & Balogh 1997; Sorriso-Valvo et al. 1999; Chhiber et al. 2018).

For these reasons, as the *Parker Solar Probe* (*PSP*; Fox et al. 2016) explores regions of the heliosphere previously inaccessible to in situ observation, several baseline questions arise concerning the observed coherent structures, whether one chooses to call them discontinuities, structures, or current sheets and vortex sheets. Since these coherent structures are routinely observed at 1 au and elsewhere, and are often found to be related to flux-tube structures, (Borovsky 2008; Neugebauer & Giacalone 2015; Zheng & Hu 2018; Pecora et al. 2019), a description of their statistical distribution along *PSP*'s orbits becomes a matter of theoretical interest as well as considerable importance in the various heliospheric plasma physics applications alluded to above. Here we make use of a simple and well-studied method for characterizing statistics of coherent structures, namely the partial variance of increments (PVI) method (Greco et al. 2009a, 2018), and apply it to characterize coherent magnetic field and velocity field structures during the first *PSP* solar encounter.

The paper is organized as follows—Section 2 defines the PVI measure and provides some background; in Section 3 we describe the data used and its processing; Sections 4 and 5 describe the results of the analyses of the magnetic and velocity PVI, respectively; we conclude with a discussion in Section 6; the Appendix discusses the association between power-law waiting times (WT) and processes that can be described as a Cantor set.

2. Background

The PVI is a well-tested measure of the occurrence of sharp gradients in the magnetic field—discontinuities, current sheets, sites of magnetic reconnection, etc. See Greco et al. (2018) for a review of applications. Such discontinuities are believed to play a key role in enhanced dissipation, and particle heating (e.g., Chasapis et al. 2015) and energization (e.g., Tessein et al. 2013) in space plasmas. If we consider a given time lag between measurements, for lags much larger than the correlation time of fluctuations, measurements of turbulent velocity and magnetic fields are typically uncorrelated and distributions of increments are Gaussian. However, for time lags corresponding to distances within the inertial range, probability density functions (PDFs) of increments have "fatter" non-Gaussian tails and are fit better by stretched exponential, lognormal, truncated Lévy-flight, and kappa distributions (Kailasnath et al. 1992; Sorriso-Valvo et al. 1999; Bruno et al. 2004; Pollock et al. 2018). Distributions of WT between high PVI "events" typically exhibit power laws at inertial range lags and exponential behavior at longer, uncorrelated lags (Greco et al. 2009b, 2018). Power-law behavior indicates a correlated "clustering" process which is statistically self-similar in time and possesses "memory," as opposed to a random Poisson process which results in exponential WT distributions. WT analyses have been employed to make this distinction in diverse fields of study, including space physics (Boffetta et al. 1999; Lepreti et al. 2001; D'Amicis et al. 2006; Greco et al. 2009b), geophysics (Carbone et al. 2006), laboratory materials (Ferjani et al. 2008), and seismology (Mega et al. 2003), to name a few.

Other studies analyzing *PSP* data (this volume) have revealed many sharp jumps in magnetic field measurements by FIELDS and proton velocity measurements by SWEAP during *PSP*'s first solar encounter (Bale et al. 2019; Horbury et al. 2020). Dudok de Wit et al. (2020) have examined statistical distributions of events identified by inspection as "switchbacks" or "jets." Examination of the same data using the PVI method represents a complementary approach, since the PVI is not tailored to a specific type of discontinuity but is instead a general tool for identifying a broad class of intermittent structures (Greco et al. 2018). Another motivation for this study lies in the fact that the PVI technique is used in two other concurrent studies in this issue of ApJS—(1) Bandyopadhyay et al. (2020b) examine the association of energetic-particle fluxes from IS⊙IS with intermittent magnetic structures, as identified by the PVI technique; (2) Qudsi et al. (2020) study the association of high proton temperatures measured by SWEAP with high magnetic-PVI values.

The PVI is essentially the magnitude of the (vector) increment in a field at a given lag, normalized by the variance of the field. Note that the increment of a turbulent field has long occupied a central role in turbulence research, with particular importance given to moments of the increment, the so-called structure functions (e.g., Monin & Yaglom 1971; Tu & Marsch 1995). The PVI is related to the first-order structure function, but is distinct in that it is a pointwise (not averaged) measure. For the magnetic field $\boldsymbol{B}$ the PVI at time s is defined, for lag τ in time, as (Greco et al. 2018):

$$\mathrm{PVI}_{s,\tau} = |\Delta \boldsymbol{B}(s,\tau)| \Big/ \sqrt{\langle |\Delta \boldsymbol{B}(s,\tau)|^2 \rangle}\,, \tag{1}$$

where the $\langle . \rangle$ denotes averaging over a suitable interval (see Isaacs et al. 2015; Krishna Jagarlamudi et al. 2019). The increment is defined as $\Delta \boldsymbol{B}(s,\tau) = \boldsymbol{B}(s+\tau) - \boldsymbol{B}(s)$. The velocity PVI is defined similarly. To compute the variance we use a moving average over a window 10 times larger than the correlation time of magnetic or velocity fluctuations, as appropriate (see Sections 4 and 5, below). Note that PVI captures gradients in each vector component of B. In the following figures, we will denote the magnetic and velocity PVI as $\mathrm{PVI}_{\boldsymbol{B}}$ and $\mathrm{PVI}_{\boldsymbol{V}}$, respectively.

Values of PVI > 3 have been associated with non-Gaussian structures, PVI > 6 with current sheets, and PVI > 8 with reconnection sites (Greco et al. 2018, and references within). Events with PVI exceeding 3 become progressively less likely to be a sample of a Gaussian random process. Therefore, even moderately large PVI selects samples of intermittency, meaning, in this context, a sample taken from the "fat tail" portion of a distribution associated with a process that admits an elevated likelihood of extreme events (Sreenivasan 1999; Matthaeus et al. 2015). Note that the PVI method is one among several that have been developed for identifying discontinuities in turbulent flows, such as the wavelet-based local intermittency measure (Veltri et al. 1999; Farge et al. 2001) and the phase coherence index (Hada et al. 2003). See the review by Greco et al. (2018) for a comparison of some of these methods with the PVI technique.

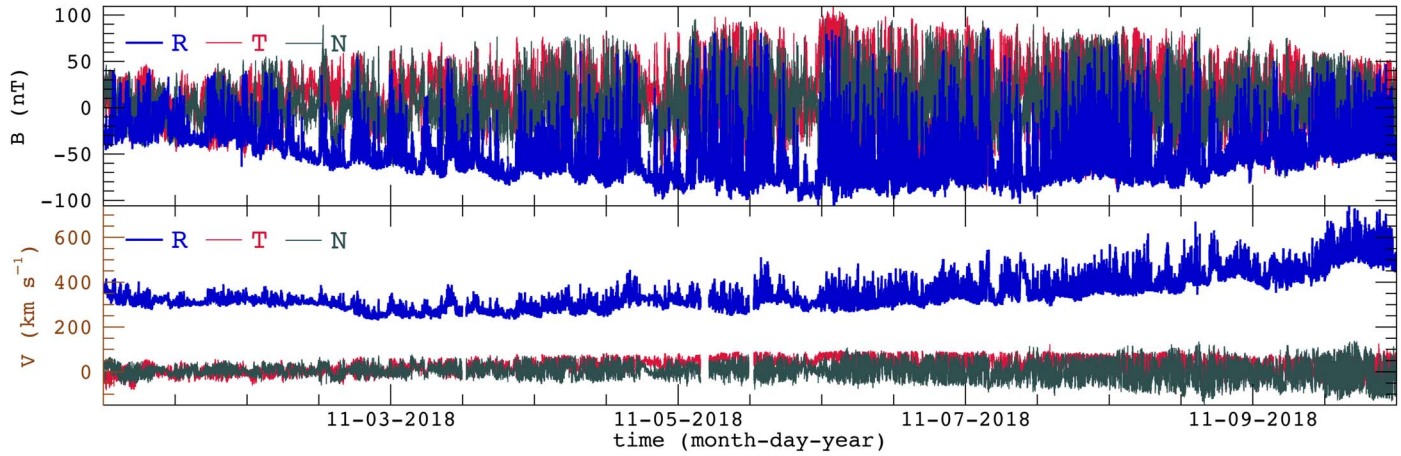

Figure 1. Time series of heliocentric RTN components (blue, red, and green curves, respectively) of magnetic and velocity fields during the period considered here are shown in the top and bottom panels, respectively. Note that the *R*-component is plotted using a thicker curve than the other two components.

Table 1

Bulk Plasma Parameters for *PSP*'s First Solar Encounter: Average Values of the Proton Speed $\langle V\rangle \equiv \langle\sqrt{V_R^2+V_T^2+V_N^2}\rangle$, Proton Temperature $\langle T_{\rm i}\rangle$, Proton Density $\langle n_{\rm i}\rangle$, Proton Inertial Scale $d_{\rm i}$, Magnetic Field Magnitude $\langle B\rangle \equiv \langle\sqrt{B_R^2+B_T^2+B_N^2}\rangle$, the rms Magnetic Fluctuation $\langle\delta B\rangle \equiv \sqrt{\langle|\boldsymbol{B}-\langle\boldsymbol{B}\rangle|^2\rangle}$, Alfvén Speed $\langle V_{\rm A}\rangle$, and Proton Beta $\beta_{\rm i}$

Time	$\langle V\rangle$	$\langle T_{\rm i}\rangle$	$\langle n_{\rm i}\rangle$	$d_{\rm i}$	$\langle B\rangle$	$\langle\delta B\rangle$	$\langle V_{\rm A}\rangle$	$\beta_{\rm i}$
2018 Nov 01 to 2018 Nov 10	350 km s^{-1}	0.6×10^6 K	215 cm^{-3}	17 km	70 nT	50 nT	100 km s^{-1}	1

Note. Averaging is performed over the entire duration of UTC time 2018-11-01T00:00:00 to 2018-11-10T23:59:59.

3. Data

We use magnetic-field data from the flux-gate magnetometer (MAG) on board the FIELDS instrument suite (Bale et al. 2016) and proton-velocity data from the Solar Probe Cup (SPC) on the SWEAP instrument suite (Kasper et al. 2016; Case et al. 2020), covering a period of about 10 days centered on the first perihelion. Bulk plasma properties over the encounter are shown in Table 1. The magnetic field data used span the full range from UTC time 2018-11-01T00:00:00 to 2018-11-09T23:59:59, and have been resampled to 1 s cadence using linear interpolation. Note that data gaps are not an issue in MAG measurements during the period considered here. The resampled magnetic data in heliocentric RTN coordinates (Fränz & Harper 2002) are shown in the top panel of Figure 1. For a detailed description of these observations, including the large "switchbacks" in the radial magnetic field, see other papers in the present volume (Bale et al. 2019; Dudok de Wit et al. 2020; Horbury et al. 2020).

We use proton velocity measurements at 0.87 s resolution from SPC, which are then processed to remove spurious or artificial spikes. These data are shown in heliocentric RTN coordinates in the bottom panel of Figure 1. Despite the numerous fluctuations, the bulk flow is fairly steady and well described as slow wind ($V_R < 500$ km s^{-1}) for most of the period considered here. During the last day *PSP* may have passed over a small coronal hole, when it sampled relatively fast wind above 600 km s^{-1}. Data gaps are a more significant issue in SPC measurements during the first encounter (compared to MAG measurements), and we have used the following procedure to prepare the data for our analyses. We first split the time series of velocity measurements from 2018 November 1 to 2018 November 10 into 8 hr long subintervals. We then discard subintervals that have data gaps larger than 10 s. The remaining subintervals have gaps with an average duration of about 1.5 s, and linear interpolation is used over these gaps. This procedure produces three periods—(i) 2018-11-01T00:00:03 to 2018-11-03T08:00:02; (ii) 2018-11-05T16:00:03 to 2018-11-07T00:00:03; and (iii) 2018-11-08T00:00:04 to 2018-11-10T08:00:03—within each of which we have continuous time series of velocity measurements at 0.87 s cadence. The PVI WT analyses are performed separately within each of these three periods, and the results are then accumulated to obtain improved statistics (see details in Section 5, below). Note that reliable WT estimation precludes the use of intervals with large data gaps.

4. PVI Analysis of the Magnetic Field

As mentioned in Section 2, to compute the PVI time series we need estimates of the correlation time of fluctuations. We use the Blackman–Tukey technique (see Matthaeus & Goldstein 1982) with an averaging interval of 24 hr to compute the autocorrelation of the magnetic field. The correlation time is estimated as the time at which the autocorrelation falls to $1/e$. Note that the correlation time does not change significantly on using a 12 hr averaging interval instead of 24 hr. The paper by Parashar et al. (2020) in the present special issue shows correlation times computed in this way for the encounter. See also Smith et al. (2001), Isaacs et al. (2015), Krishna Jagarlamudi et al. (2019), and Bandyopadhyay et al. (2020a) for discussions of subtleties and potential issues in accurate determination of correlation times. An alternative estimate of the correlation time may be obtained from the break frequency between "$1/f$" (Matthaeus & Goldstein 1986) and inertial ranges in the power spectrum of magnetic fluctuations (Chen et al. 2020, present volume); we confirmed that this estimate is comparable to the correlation time we use here. Furthermore, the PVI does not appear to depend sensitively on the averaging interval used.

During the period analyzed here the magnetic correlation time varies from about 350 s to 1000 s. Accordingly, assuming

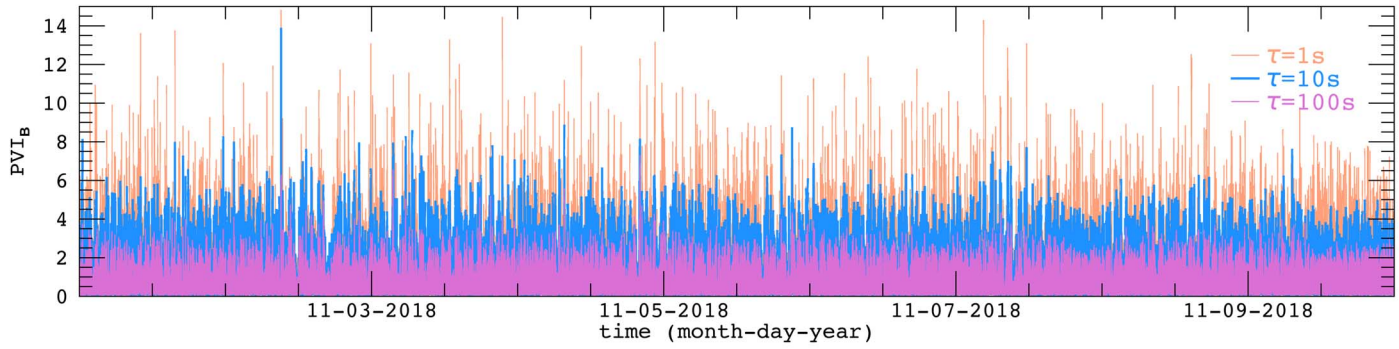

(a)

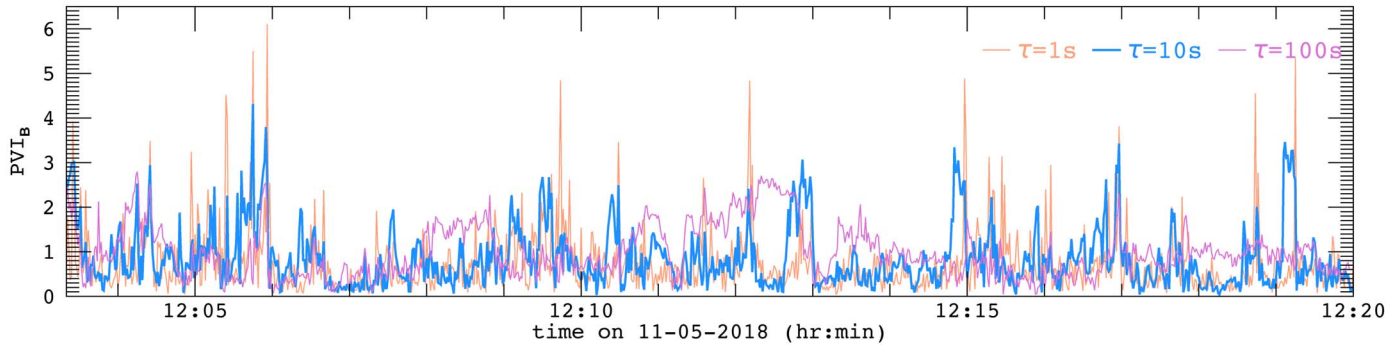

(b)

Figure 2. (a) PVI (with lag τ equal to 1, 10, and 100 s) time series for magnetic field during the first encounter. (b) The same time series for about 15 minutes on 2018 November 5. In both panels the 10 s case is shown as a thicker line compared to the other two.

an average correlation time of 600 s for the encounter, we use a rolling boxcar average over a window 10×600 s in duration to estimate the variance (the denominator in Equation (1)) for computation of magnetic PVI. The resulting time series is shown in Figure 2 for three different lags: $\tau = 1$, 10, and 100 s. The 1 and 10 s lags lie well within the inertial range (the ion inertial scale corresponds to an approximate temporal lag of 0.05 s (Parashar et al. 2020), while the 100 s lag is comparable to the correlation time. Note that as the lag τ is increased we still sample over times with 1 s cadence.

It is clear from Figure 2 that at smaller lags the PVI measure captures highly intermittent events, while such events are relatively rare in the time series computed using a 100 s lag. This is reinforced by Figure 3, which shows histograms of PVI for the three lags. The most probable value of PVI is about 0.5 for all three cases, and corresponds to the majority of events, which are, by definition, nonintermittent. While all three lags capture a large number of non-Gaussian (PVI > 3) events, the tails of the histograms become wider as the lag is decreased; the 1 and 10 s lags pick out hundreds of current sheets (PVI > 6), and possible reconnection sites (PVI > 8) are detected with 1 s lag.

In Figure 4 we present the main results of this work—PDFs of WT between intermittent PVI events with varying lag and threshold. Here the WT between two events is defined as the time between the end of the first event and the beginning of the second event. Note that the events may have finite duration; i.e., if the PVI stays above the threshold for consecutive times then these times are regarded as part of the same event. Power-law and exponential fits (based on chi-squared error minimization) to the PDFs are also shown, and the average WT computed from the

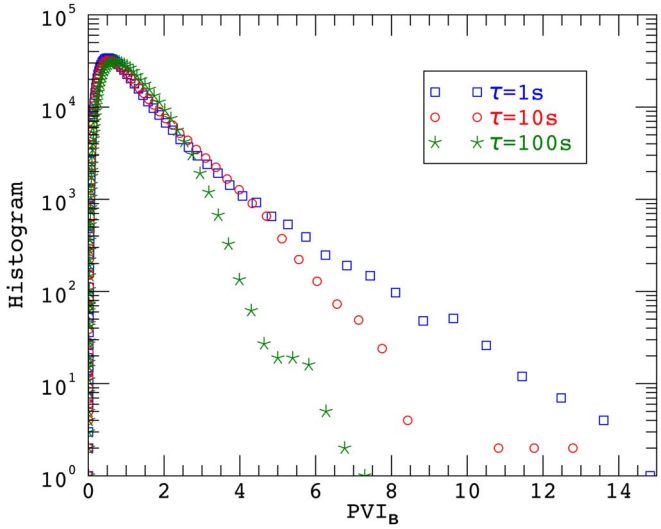

Figure 3. Histograms (showing frequency of occurrence, or number of counts) of PVI values for different lags τ, for the magnetic field during the first encounter. Note the elevated likelihood of large PVI values at shorter lags, indicative of enhanced small-scale intermittency, typical of non-Gaussian processes and turbulence.

distribution are indicated as $\langle \mathrm{WT} \rangle$. Uncertainties in fit parameters and goodness-of-fit estimates are also reported in the caption.

It is apparent from all four panels of Figure 4 that the distribution of WT is well described as a power law for events whose temporal separation is smaller than the correlation time, suggesting strong correlation and clustering. For events that are farther apart in time, the distribution is better fit by an

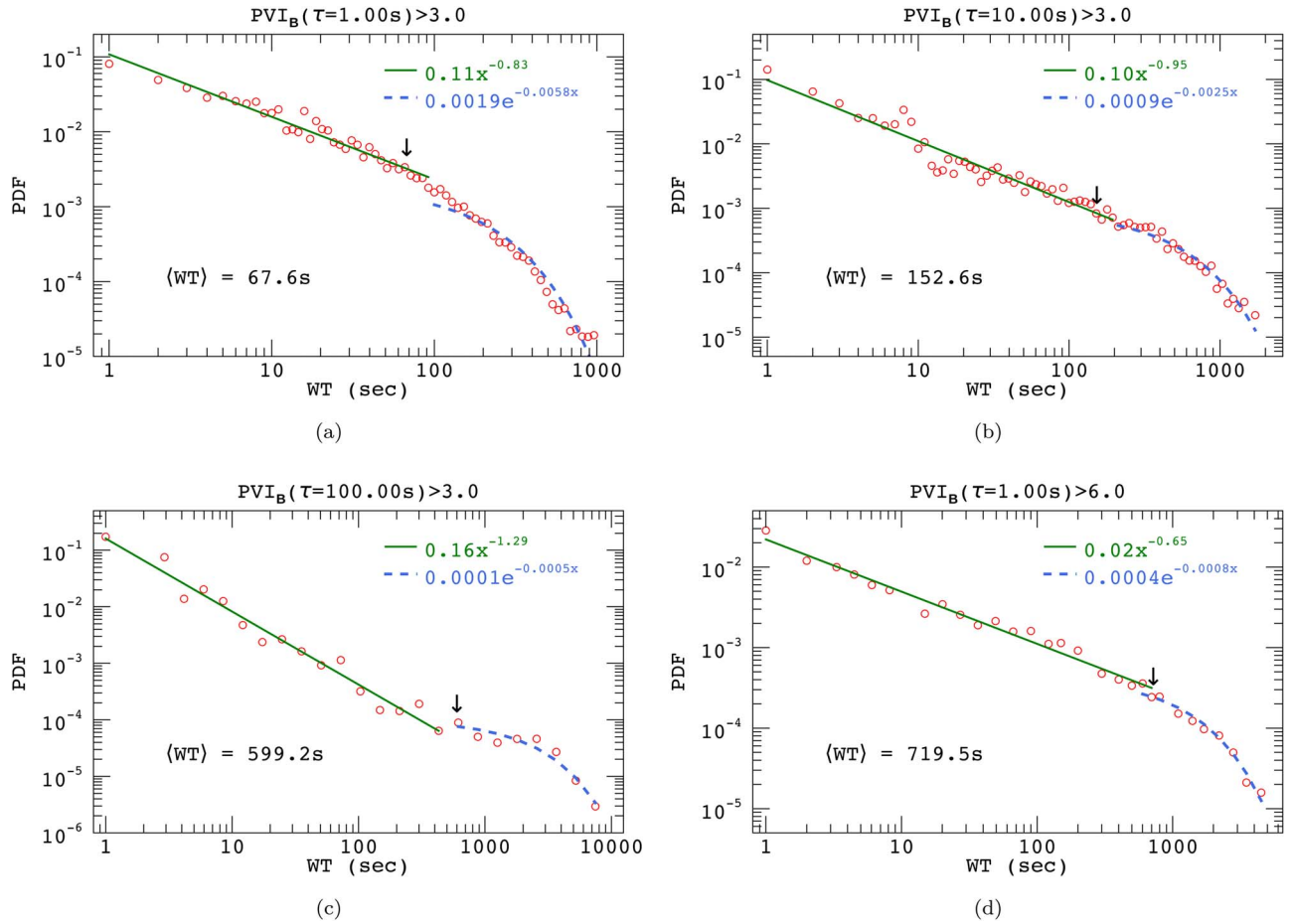

Figure 4. PDFs of WT between magnetic PVI > 3 events for lags τ equal to (a) 1, (b) 10, and (c) 100 s. Panel (d) shows the PDF of WT between magnetic PVI > 6 events for 1 s lag. Bins with fewer than 10 counts have been discarded, except in (c) where bins with fewer than 5 counts have been discarded. The average waiting times $\langle \mathrm{WT} \rangle$ are also indicated, with downward arrows marking their location on the horizontal axes. Power-law fits ($\beta\, x^{\alpha}$) are shown as solid green lines and exponential fits ($\gamma\, e^{-\delta x}$) as dashed blue curves; here x refers to the WT. 1σ uncertainty estimates for fit parameters $\{\beta, \alpha, \gamma, \delta\}$ for the four panels are, respectively: (a) {0.01, 0.03, 0.0002, 0.0003}; (b) {0.01, 0.04, 8.8e-05, 0.0001}; (c) {0.04, 0.06, 1.8e-05, 4.8e-05}; and (d) {0.002, 0.02, 4.8e-05, 4.9e-05}. Pearson correlation coefficients, indicating goodness-of-fit for the power-law fits, are above 0.95 for each panel.

exponential, indicative of a random Poisson-type process (Greco et al. 2009b). In fact, the break between the power-law and exponential regimes is associated with the average WT. While acknowledging that these power-law distributions lack a well-defined average (Newman 2005), we might interpret $\mathrm{WT} < \langle \mathrm{WT} \rangle$ to be an intracluster WT, and $\mathrm{WT} > \langle \mathrm{WT} \rangle$ as an intercluster WT. The latter is consistent with an exponential, so WT between clusters is governed by a uniform random Poisson process. Within clusters, there is strong correlation. We remark here that truncated Lévy-flight (TLF) distributions include both a power-law range along with an exponential cutoff (Bruno et al. 2004, and references within), and in future work it would be worth examining the present results in the context of such TLFs.

Another feature of interest in Figure 4 is the small spike in the PDF near $\mathrm{WT} = \tau$, suggesting that the PVI at a given lag may preferentially pick out events with a characteristic WT equal to the specified lag.[18] We also note that the magnitude of the slope α of the power law systematically increases with increasing lag, indicating a weakening of the clusterization (see the Appendix). Furthermore, for $\tau = 1$, the slope is shallower for the case of the PVI > 6 threshold compared to the PVI > 3 threshold, suggesting that more intermittent events are more strongly clustered. Note that we have not examined longer lags for the PVI > 6 threshold, since such high PVI values are relatively rare for 10 and 100 s lags (see Figure 3). We remark here that we also performed this analysis for the periods of 2018 October 17–26 and 2018 November 14–24, and obtained similar results.

In Table 2 we show power-law slopes, average WT, and average durations of events for the various lags and thresholds considered here. Times have also been converted to distances assuming Taylor's hypothesis (Taylor 1938) with a constant average radial speed of 350 km s^{-1} for the encounter.[19] Note that the Taylor hypothesis has been found to have reasonable

[18] This appears to be a general property of the PVI measure that can be seen in previous work (e.g., see Figure 4 in Greco et al. 2009b), but has either not been noticed or not remarked upon until now. As a tentative explanation, imagine a single data point with a strong fluctuation relative to its neighbors, and suppose the lag is 100 s. Then, 100 s before this point there is a strong likelihood of a PVI event, and of another PVI event at the time of this point. This could lead to an increased chance of $\mathrm{WT} = \tau$ compared to neighboring values of WT.

[19] Since *PSP* and the solar wind plasma were in near-corotation near perihelion (Kasper et al. 2019), we reasoned that the plasma was convecting past the spacecraft primarily in the radial direction, and therefore used the radial speed of the solar wind while employing the Taylor hypothesis. For discussions of "alternative" Taylor's hypotheses that are being examined for use with *PSP* data, see, e.g., Matthaeus (1997), Klein et al. (2015), Matthaeus et al. (2016), Bourouaine & Perez (2018), Chhiber et al. (2019), and Bourouaine & Perez (2019).

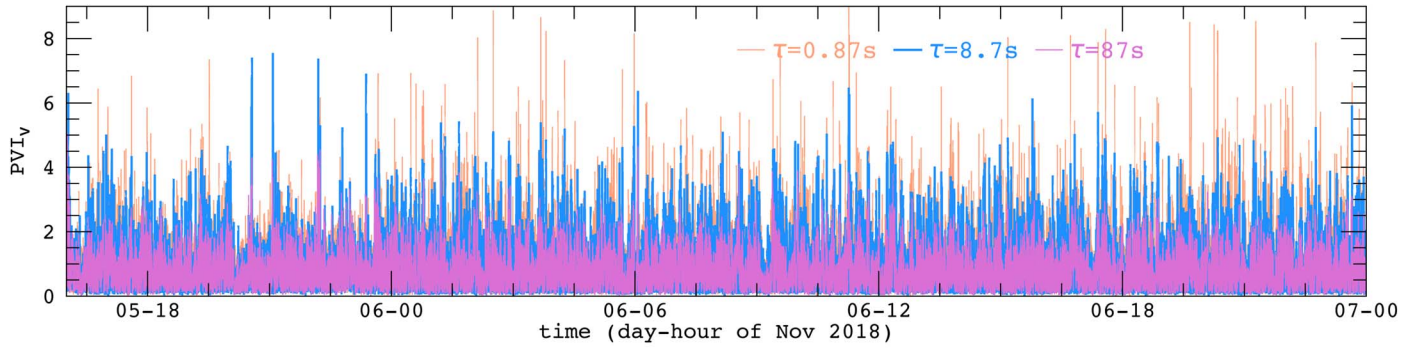

(a)

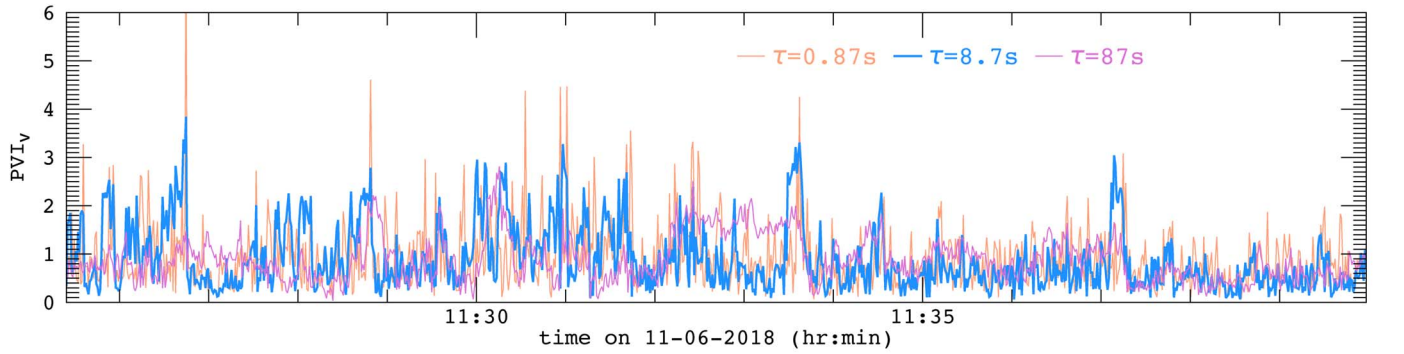

(b)

Figure 5. (a) PVI (with lag τ equal to 0.87, 8.7, and 87 s) time series for the proton velocity from UTC 2018-11-05T16:00:03 to 2018-11-07T00:00:03, including the first perihelion. (b) The same time series for about 15 minutes on 2018 November 6. In both panels the 8.7 s case is shown as a thicker line compared to the other two.

Table 2
Power-law Indices α of Fits to WT Distributions, Mean Waiting-times $\langle WT \rangle$ in s, and Mean Durations $\langle T_{dur} \rangle$ in s, for Different PVI lags (τ) and Thresholds, for the Magnetic Field

	$PVI_B > 3$			$PVI_B > 6$		
τ in s (km)	α	$\langle WT \rangle$ in s (km)	$\langle T_{dur} \rangle$ in s (km)	α	$\langle WT \rangle$ in s (km)	$\langle T_{dur} \rangle$ in s (km)
1 (350)	−0.83	67.6 (23,000)	1.2 (420)	−0.65	719.5 (252,000)	1.0 (350)
10 (3500)	−0.95	152.6 (53,000)	2.7 (945)			
100 (35,000)	−1.29	599.2 (210,000)	4.5 (1575)			

Note. Times have been converted to approximate characteristic distances (shown in kilometers in parentheses) assuming Taylor's hypothesis with an average radial speed of 350 km s^{-1} (see the discussion in the text). For reference, the mean correlation time (distance) for magnetic fluctuations during the encounter is about 600 s (200,000 km). Above $\langle WT \rangle$ the WT depart from a power law and follow an exponential distribution.

validity during the first encounter (see Chen et al. 2020; Parashar et al. 2020), consistent with predictions based on turbulence modeling of the solar wind (Chhiber et al. 2019). However, the distances shown in Table 2 should be considered crude estimates, in view of the observed variations in radial velocity (Figure 1) relative to the mean used here. Note that this constant radial speed is used only in estimations of characteristic distances, and plays no role in our temporal analyses and conclusions (see, however, the discussion in Section 6 on possible differences in WT statistics between slow and fast wind).

5. PVI Analysis of Velocity

Next we present results of the PVI WT analysis for proton velocity. As discussed in Section 3, data gaps are a more significant issue for velocity measurements by the SPC, compared with MAG data. Velocity-data selection and processing are described in Section 3. The resulting subsamples (i), (ii), and (iii) have velocity correlation times of 1700, 325, and 700 s, respectively, and a rolling average over an interval 10 times larger than these times is employed for computing the PVI time series (Equation (1)). The time series for the second subsample (including the perihelion) is shown in Figure 5, for three different lags. As in the case of the magnetic field, smaller lags detect more intermittent events, although there appear to be relatively fewer events with very high velocity–PVI. This finding is reinforced by the histograms shown in Figure 6, with the caveat that the volume of data used in the analyses for the velocity is smaller than that for the magnetic field, since in the former case only intervals that survive the data-selection procedure (Section 3) are used. Nevertheless, we do find thousands of non-Gaussian events (PVI > 3) and more than a hundred possible current sheets (PVI > 6).

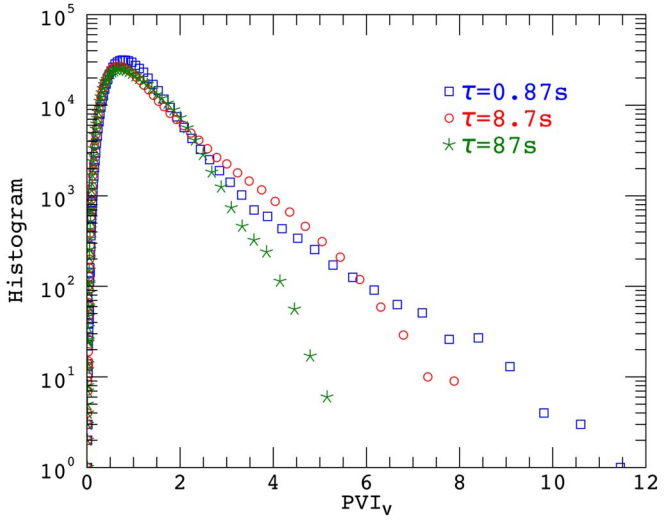

Figure 6. Histograms (showing frequency of occurrence, or number of counts) of PVI values for different lags τ, for the proton velocity during the first encounter. Note the elevated likelihood of large PVI values at shorter lags, indicative of enhanced small-scale intermittency, typical of non-Gaussian processes and turbulence.

Moving on to distributions of WT between velocity PVI events, the results in Figure 7 are consistent with the magnetic case (Figure 4). The PDFs are well described by power laws up to the average WT, and are fit better by exponentials for larger WT. Once again this behavior suggests strong correlations within clusters of size $\langle \mathrm{WT} \rangle$, and random Poisson intercluster processes. The magnitude of slope α of the power law increases with increasing lag, and, for the 0.87 s lag, the slope of the PVI > 6 power law is shallower than the PVI > 3 case, suggesting once again that stronger intermittency is associated with increased clusterization. The small spike in the PDF at WT $= \tau$ is also seen here.

Table 3 shows power-law slopes, average WT, and average durations of PVI events for the various lags and thresholds considered. Times have been converted to approximate characteristic distances assuming Taylor's hypothesis with a constant speed of 350 km s^{-1}, as in the magnetic case.

6. Conclusions and Discussion

In this paper we have employed the PVI methodology to provide a baseline statistical characterization of the "roughness", or intermittency, of the observed magnetic and velocity field during the first solar encounter of the *PSP*. Quantification of roughness using the PVI technique has the dual advantages of being closely related to turbulence intermittency statistics, while also being related to classical-discontinuity identification procedures (Greco et al. 2009b, 2018, and references within).[20] The present work extends in a natural way analogous studies carried out at 1 au and beyond (Greco et al. 2018, and references within). Values of PVI above appropriate thresholds have been found to be related to classical discontinuities (Greco et al. 2008, 2009b), intermittency and current sheets (Greco et al. 2009a; Servidio et al. 2011; Malaspina et al. 2013; Osman et al. 2014), particle energization (Tessein et al. 2013, 2015, 2016), kinetic effects such as elevated temperature and high degrees of non-Guassianity in the velocity distribution function (Osman et al. 2011, 2012; Servidio et al. 2015; Qudsi et al. 2020), and, at high PVI, likelihood of magnetic reconnection (Servidio et al. 2011). In this sense it is a natural follow-on to examine whether those tendencies extend further into the inner heliosphere than has been previously explored. However, additional motivation is obtained through early reports that the magnetic and velocity fields near *PSP* perihelion exhibit strong "jets" or "switchbacks" that may suggest enhanced, episodic, and large-amplitude quasi-discontinuous jumps in plasma conditions (see several papers in this special volume). PVI seems to be an appropriate general tool for broadly identifying and quantifying such intermittent structure. Note that a further detailed study of specific types of structures, such as the observed "switchbacks," requires a more specialized approach (see Dudok de Wit et al. 2020).

Our main results are summarized in Tables 2 and 3. During the first *PSP* encounter, fluctuations of both the magnetic field and the velocity exhibit statistical features, specifically inter-event WT distributions, that suggest the appearance of both correlated as well as random or Poissonian events. Such events are interpreted as non-Gaussian coherent structures, consistent with current sheets and vortex sheets. The presence of these signals may be related to interpretations based on intermittent turbulence, although the method itself is also sensitive to classical discontinuities. For WT shorter than about a correlation scale, the presence of power-law distributions indicates correlations and is suggestive of clustering. In the Appendix we consider an analogy with generalized self-similar Cantor sets, for which the power-law index α ranges from -2 to -1 with increasing clustering. For WT larger than about the measured correlation scales, the exponential distribution of WT indicates uncorrelated random events. The clustering appears to weaken with increasing PVI lag, and, for the same lag, more intermittent events are more strongly clustered. This behavior is consistently seen in both magnetic and velocity fields, which is perhaps not surprising given the high Alfvénicity of the fluctuations observed during the encounter (Bale et al. 2019; Chen et al. 2020; Parashar et al. 2020). Our results complement those of Dudok de Wit et al. (2020), who find that WT between the observed "switchbacks" in the radial magnetic field are well described by power laws.

These findings appear to be consistent with some recent studies of near-Earth solar-wind fluctuations (Greco et al. 2009b), as well as simulations of MHD turbulence (Greco et al. 2008). Note that the correlation time increases as one moves outward toward 1 au (Breech et al. 2008; Bruno & Carbone 2013; Ruiz et al. 2014; Zank et al. 2017) and the turbulence "ages" (Matthaeus et al. 1998); therefore, one expects the shift from power-law to exponential behavior to occur at larger WT compared to the present results for the young solar wind. Indeed, here we find average WT of about 3–10 minutes, which are smaller than the typical values of 30–50 minutes seen at 1 au (Tsurutani & Smith 1979; Bruno et al. 2001; Greco et al. 2008). Note that other studies have found exponential WT distributions for intermittent events in near-Earth (and beyond) solar wind (Tsurutani & Smith 1979; Bruno et al. 2001), without a power-law regime. Interestingly, Hu et al. (2018) find power-law distributions at longer WT ($>$ 60 minutes) and exponential behavior before that, for

[20] By "classical discontinuity" we are referring to the traditional interpretation of (mostly magnetic) discontinuities in the solar wind as members of a class of MHD stationary convected structures (such as tangential discontinuities) or propagating rotational discontinuities, which are viewed as static solutions of the ideal MHD equations (e.g., Neugebauer & Giacalone 2010).

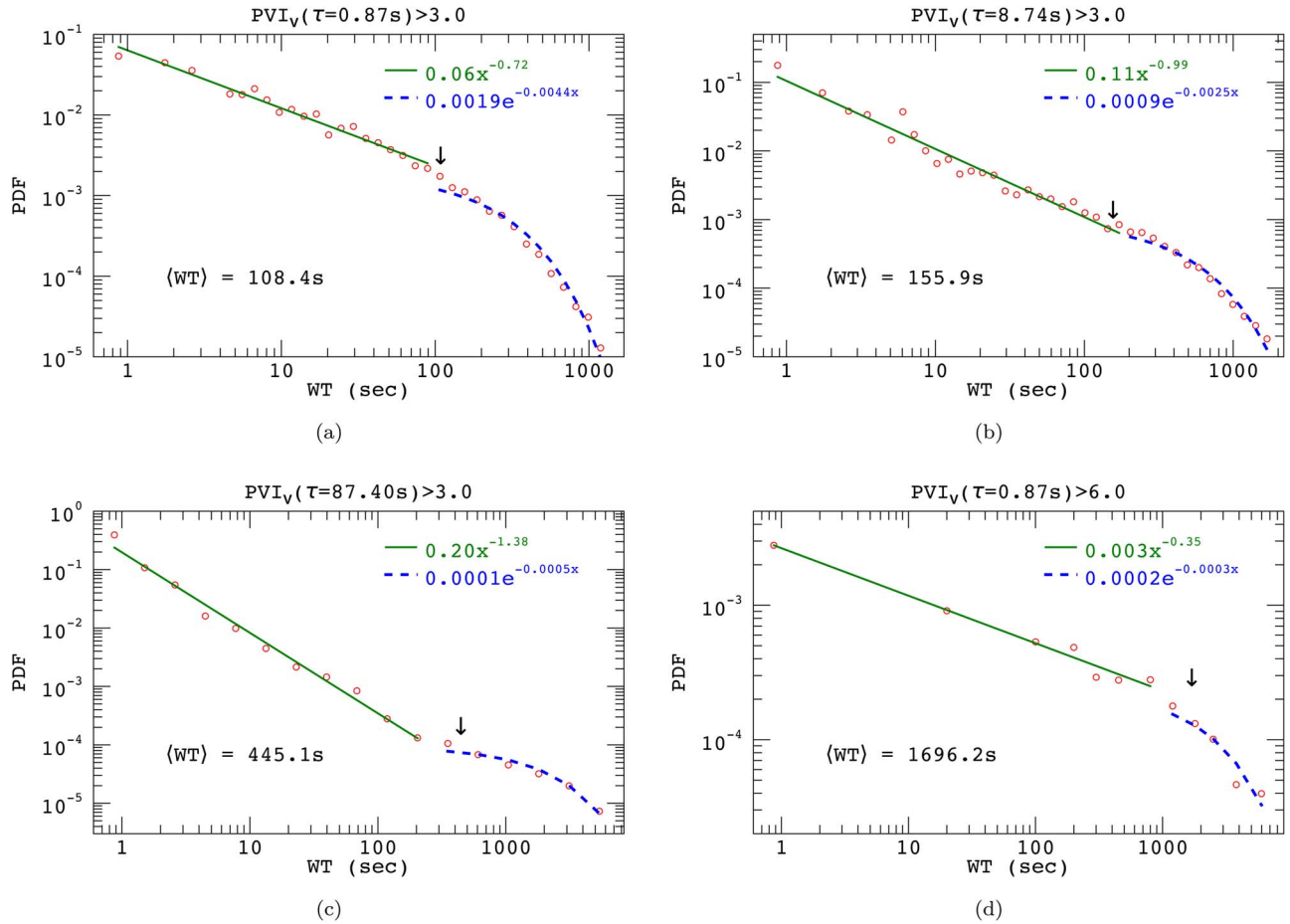

Figure 7. PDFs of WT between (proton) velocity PVI > 3 events for PVI lags (a) 0.87, (b) 8.7, and (c) 87 s. Panel (d) shows the PDF of WT between (proton) velocity PVI > 6 events for 0.87 s lag. Bins with fewer than 10 counts have been discarded in panels (a)–(c), while in panel (d) bins with fewer than 5 counts have been discarded. The average waiting times $\langle \mathrm{WT} \rangle$ are also indicated, with downward arrows marking their locations on the horizontal axes. Power-law fits ($\beta\, x^{\alpha}$) are shown as solid green lines and exponential fits ($\gamma\, e^{-\delta\, x}$) as dashed blue curves; here x refers to the WT. 1σ uncertainty estimates for fit parameters $\{\beta,\ \alpha,\ \gamma,\ \delta\}$ for the four panels are, respectively: (a) {0.005, 0.03, 0.0002, 0.0002}; (b) {0.01, 0.04, 0.0001, 0.0001}; (c) {0.03, 0.05, 1.2e-05, 4.9e-05}; and (d) {0.0003, 0.02, 5.3e-05, 6.6e-05}. Pearson correlation coefficients indicating goodness-of-fit for the power-law fits are above 0.95 for each panel.

Table 3
Power-law Indices α of fit to WT Distributions, Mean Waiting Times $\langle \mathrm{WT} \rangle$ in s, and Mean Durations $\langle \mathrm{T_{dur}} \rangle$ in s, for Different PVI Lags (τ) and Thresholds, for the Proton Velocity

	$\mathrm{PVI}_V > 3$			$\mathrm{PVI}_V > 6$		
τ in s (km)	α	$\langle \mathrm{WT} \rangle$ in s (km)	$\langle \mathrm{T_{dur}} \rangle$ in s (km)	α	$\langle \mathrm{WT} \rangle$ in s (km)	$\langle \mathrm{T_{dur}} \rangle$ in s (km)
0.87 (305)	−0.72	108.4 (38,000)	0.98 (343)	−0.35	1696.2 (594,000)	0.89 (312)
8.7 (3045)	−0.99	155.9 (55,000)	2.3 (805)			
87 (30,450)	−1.38	445.1 (156,000)	3.2 (1120)			

Note. Times have been converted to distances (shown in kilometers in parentheses) assuming Taylor's hypothesis with an average radial speed of 350 km s^{-1}. For reference, the mean correlation time (distance) for velocity fluctuations near perihelion is about 325 s (114,000 km). Above $\langle \mathrm{WT} \rangle$ the WT depart from a power law and follow an exponential distribution.

small-scale flux ropes identified using a Grad–Shafranov reconstruction technique with *Wind* observations (see, however, Zheng & Hu 2018). Assuming wind speed as the sole criterion for classification, the current *PSP* observations are mostly restricted to slow-wind conditions in the ecliptic during solar minimum. Future orbits are expected to sample extended periods of fast wind as well, and it will be interesting to compare WT statistics between slow and fast wind in the near-Sun plasma. Farther away, *Helios* observations find power-law behavior up to longer WT in the case of slow wind compared with fast wind (D'Amicis et al. 2006). In future work it would also be interesting to use full-cadence MAG data (or search-coil magnetometer measurements) from *PSP* to probe PVI events at kinetic-scale lags.

The dichotomy between a strongly correlated clustering process and a random Poissonian process may be related to two contrasting views of the origin of magnetic structures in the solar wind—in situ generation via turbulent cascade versus passive advection from the solar source. The strong clustering seen in our present results readily leads to the suggestion that

these observed features may originate in a hierarchy of nonlinear processes that generate correlations of nearby structures over a broad range of scales. Our preferred explanation is strong turbulence occurring in the corona and/or interplanetary medium. Turbulence is known to produce these features, as has been observed routinely in space plasmas including the solar wind and the terrestrial magnetosheath (Yordanova et al. 2008; Matthaeus & Velli 2011; Bruno & Carbone 2013; Greco et al. 2018). The unique feature of the present analysis is finding these indicators of intermittency and turbulence at distances closer to the Sun, and therefore closer to source and boundary surfaces, than has been accomplished in any previous space mission. This may eventually produce constraints on how turbulence is initiated in the inner heliosphere, or how it is transmitted and propagated from the corona into the super-Alfvénic solar wind. Fully satisfactory answers to such questions will likely require additional complementary observations by *PSP* in subsequent orbits, and by the upcoming Solar Orbiter mission. Furthermore, it is likely that more complete interpretations will require context support from global heliospheric simulations to establish likely connections between in situ observation and remote sensing of the inner solar atmosphere, for example, by Solar Orbiter or by the upcoming PUNCH mission.

This research as been supported in part by the *Parker Solar Probe* mission under the IS⊙IS project (contract NNN06AA01C) and a subcontract to University of Delaware from Princeton (SUB0000165). Additional support is acknowledged from NASA's LWS (NNX17AB79G), HSR (80NSSC18K1210 and 80NSSC18K1648), and HGI (80NSSC19K0284) programs; and grant RTA6280002 from Thailand Science Research and Innovation. *Parker Solar Probe* was designed, built, and is now operated by the Johns Hopkins Applied Physics Laboratory as part of NASA's Living with a Star (LWS) program (contract NNN06AA01C). Support from the LWS management and technical team has played a critical role in the success of the *Parker Solar Probe* mission.

Appendix
Waiting Times for the Cantor Set

Here we provide details of the association between power-law WT and processes or structures that can be described by a Cantor set.

For a given power-law distribution of WT, with PDF $\propto \mathrm{WT}^{\alpha}$, it may not be clear how to physically interpret the power-law index α. Intuitively, it seems that a harder distribution should indicate stronger clustering than a softer distribution, i.e., $\alpha \approx -1$ should indicate stronger clustering than $\alpha \approx -2$, because a process with a harder WT distribution more frequently has a long hiatus followed by numerous events in rapid succession.

To interpret α more quantitatively, and given that (statistical) self-similarity is a common feature of inertial range turbulence, we consider the WT distribution of the Cantor set (Smith 1874; Cantor 1883). Recall that this set is defined as the points remaining after an infinite sequence of operations: At stage $n = 0$ we start with the set [0, 1], then in stage $n = 1$ we remove the middle one-third with two segments remaining at either side, and in each subsequent stage n we remove the middle $1/3$ of each remaining segment, doubling the number of remaining segments to become 2^n. If the "waiting time" T is defined as the distance between successive points in the Cantor set, then all WT are $T_n = 3^{-n}$ for some $n \in \{1, 2, 3, \ldots\}$, and the number of WT generated in stage n is $N_n = 2^{n-1}$. An unnormalized PDF of WT can be defined as $N_n/(T_n - T_{n+1})$, which results in

$$\mathrm{PDF}(T_n = 3^{-n}) = \frac{2^{n-1}}{(2/3)3^{-n}} = \frac{9}{2}6^{n-1}. \tag{2}$$

This implies that

$$\alpha = \frac{\ln\mathrm{PDF}(T_{n+1}) - \ln\mathrm{PDF}(T_n)}{T_{n+1} - T_n} = -\frac{\ln 6}{\ln 3} \approx -1.631. \tag{3}$$

(The same power-law index results if we instead define the PDF from $N_n/(T_{n-1} - T_n)$.) Remarkably, some of the present observational results for PVI events have α close to -1, implying that large field increments in the solar wind can be more strongly clustered than the Cantor set. Similar slopes have been observed near 1 au (Greco et al. 2009b).

As a generalization of the Cantor set, consider a set in which at each stage, instead of removing one-third of each segment, we remove a fraction f of the segment from the middle. As $f \to 1$, more of the segment is removed and the remaining points are more clustered with wider gaps. Each remaining segment after $n = 1$ has a size $(1 - f)/2$, and after stage n the segment size is $[(1 - f)/2]^n$. Then $T_n = f[(1 - f)/2]^{n-1}$ and we still have $N_n = 2^{n-1}$, so

$$\begin{aligned}\mathrm{PDF}(T_n) &= \frac{2^{n-1}}{f[(1+f)/2][(1-f)/2]^{n-1}} \\ &= \frac{2}{f(1+f)}\left(\frac{4}{1-f}\right)^{n-1}\end{aligned} \tag{4}$$

and

$$\alpha = \frac{\ln[4/(1-f)]}{\ln[(1-f)/2]} = -\frac{2\ln 2 - \ln(1-f)}{\ln 2 - \ln(1-f)}. \tag{5}$$

For $0 < f < 1$, we have $-2 < \alpha < -1$, with $\alpha \to -1$ as $f \to 1$. Thus our observation of $\alpha \approx -1$ for field increments in the solar wind implies extreme clustering, equivalent to the maximum clustering possible for such a generalized Cantor set.

ORCID iDs

Rohit Chhiber https://orcid.org/0000-0002-7174-6948
M L. Goldstein https://orcid.org/0000-0002-5317-988X
B. A. Maruca https://orcid.org/0000-0002-2229-5618
A. Chasapis https://orcid.org/0000-0001-8478-5797
W. H. Matthaeus https://orcid.org/0000-0001-7224-6024
D. Ruffolo https://orcid.org/0000-0003-3414-9666
R. Bandyopadhyay https://orcid.org/0000-0002-6962-0959
T. N. Parashar https://orcid.org/0000-0003-0602-8381
R. Qudsi https://orcid.org/0000-0001-8358-0482
T. Dudok de Wit https://orcid.org/0000-0002-4401-0943
S. D. Bale https://orcid.org/0000-0002-1989-3596
J. W. Bonnell https://orcid.org/0000-0002-0675-7907
R. J. MacDowall https://orcid.org/0000-0003-3112-4201
D. Malaspina https://orcid.org/0000-0003-1191-1558
M. Pulupa https://orcid.org/0000-0002-1573-7457
J. C. Kasper https://orcid.org/0000-0002-7077-930X
K. E. Korreck https://orcid.org/0000-0001-6095-2490
A. W. Case https://orcid.org/0000-0002-3520-4041

P. Whittlesey https://orcid.org/0000-0002-7287-5098
D. Larson https://orcid.org/0000-0001-5030-6030
R. Livi https://orcid.org/0000-0002-0396-0547
M. Velli https://orcid.org/0000-0002-2381-3106

References

Bale, S., Badman, S. T., Bonnell, J. W., et al. 2019, Natur, 576, 237
Bale, S. D., Goetz, K., Harvey, P. R., et al. 2016, SSRv, 204, 49
Bandyopadhyay, R., Goldstein, M. L., Maruca, B. A., et al. 2020a, ApJS, doi:10.3847/1538-4365/ab5dae
Bandyopadhyay, R., Matthaeus, W. H., Parashar, T. N., et al. 2020b, ApJS, doi:10.3847/1538-4365/ab6220
Biskamp, D. 2003, Magnetohydrodynamic Turbulence (Cambridge: Cambridge Univ. Press)
Boffetta, G., Carbone, V., Giuliani, P., Veltri, P., & Vulpiani, A. 1999, PhRvL, 83, 4662
Borovsky, J. E. 2008, JGRA, 113, A08110
Bourouaine, S., & Perez, J. C. 2018, ApJL, 858, L20
Bourouaine, S., & Perez, J. C. 2019, ApJL, 879, L16
Breech, B., Matthaeus, W. H., Minnie, J., et al. 2008, JGRA, 113, A08105
Bruno, R., & Carbone, V. 2013, LRSP, 10, 2
Bruno, R., Carbone, V., Veltri, P., Pietropaolo, E., & Bavassano, B. 2001, P&SS, 49, 1201
Bruno, R., Sorriso-Valvo, L., Carbone, V., & Bavassano, B. 2004, EL, 66, 146
Burlaga, L. F., & Ness, N. F. 1969, SoPh, 9, 467
Cantor, G. 1883, MatAn, 21, 545
Carbone, V., Sorriso-Valvo, L., Vecchio, A., et al. 2006, PhRvL, 96, 128501
Case, A. C., Kasper, J. C., Stevens, M. L., et al. 2020, ApJS, doi:10.3847/1538-4365/ab5a7b
Chasapis, A., Retinò, A., Sahraoui, F., et al. 2015, ApJL, 804, L1
Chen, C. H. K., Bale, S. D., Bonnell, J. W., et al. 2020, ApJS, doi:10.3847/1538-4365/ab60a3
Chhiber, R., Chasapis, A., Bandyopadhyay, R., et al. 2018, JGRA, 123, 9941
Chhiber, R., Usmanov, A. V., Matthaeus, W. H., Parashar, T. N., & Goldstein, M. L. 2019, ApJS, 242, 12
D'Amicis, R., Bruno, R., Bavassano, B., Carbone, V., & Sorriso-Valvo, L. 2006, AnGeo, 24, 2735
Dudok de Wit, T., Krasnoselskikh, V. V., Bale, S. D., et al. 2020, ApJS, doi:10.3847/1538-4365/ab5853
Farge, M., Pellegrino, G., & Schneider, K. 2001, PhRvL, 87, 054501
Ferjani, S., Sorriso-Valvo, L., de Luca, A., et al. 2008, PhRvE, 78, 011707
Fox, N. J., Velli, M. C., Bale, S. D., et al. 2016, SSRv, 204, 7
Fränz, M., & Harper, D. 2002, P&SS, 50, 217
Frisch, U. 1995, Turbulence. The Legacy of A. N. Kolmogorov (Cambridge: Cambridge Univ. Press)
Greco, A., Chuychai, P., Matthaeus, W. H., Servidio, S., & Dmitruk, P. 2008, GeoRL, 35, L19111
Greco, A., Matthaeus, W. H., Perri, S., et al. 2018, SSRv, 214, 1
Greco, A., Matthaeus, W. H., Servidio, S., Chuychai, P., & Dmitruk, P. 2009a, ApJL, 691, L111
Greco, A., Matthaeus, W. H., Servidio, S., & Dmitruk, P. 2009b, PhRvE, 80, 046401
Greco, A., Valentini, F., Servidio, S., & Matthaeus, W. H. 2012, PhRvE, 86, 066405
Hada, T., Koga, D., & Yamamoto, E. 2003, SSRv, 107, 463
Hellinger, P., Verdini, A., Landi, S., Franci, L., & Matteini, L. 2018, ApJL, 857, L19
Horbury, T. S., & Balogh, A. 1997, NPGeo, 4, 185
Horbury, T. S., Woolley, T., Laker, R., et al. 2020, ApJS, doi:10.3847/1538-4365/ab5b15
Hu, Q., Zheng, J., Chen, Y., le Roux, J., & Zhao, L. 2018, ApJS, 239, 12
Isaacs, J. J., Tessein, J. A., & Matthaeus, W. H. 2015, JGRA, 120, 868
Kailasnath, P., Sreenivasan, K. R., & Stolovitzky, G. 1992, PhRvL, 68, 2766
Karimabadi, H., Roytershteyn, V., Wan, M., et al. 2013, PhPl, 20, 012303
Kasper, J. C., Abiad, R., Austin, G., et al. 2016, SSRv, 204, 131
Kasper, J. C., Bale, S. D., Belcher, J. W., et al. 2019, Natur, 576, 228
Klein, K. G., Perez, J. C., Verscharen, D., Mallet, A., & Chandran, B. D. G. 2015, ApJL, 801, L18
Krishna Jagarlamudi, V., Dudok de Wit, T., Krasnoselskikh, V., & Maksimovic, M. 2019, ApJ, 871, 68
Lepreti, F., Carbone, V., & Veltri, P. 2001, ApJL, 555, L133
Malaspina, D. M., Newman, D. L., Wilson, L. B. I., et al. 2013, JGRA, 118, 591
Matthaeus, W. H. 1997, in AIP Conf. Ser. 385, Robotic Exploration Close to the Sun: Scientific Basis, ed. S. R. Habbal (Melville, NY: AIP), 67
Matthaeus, W. H., & Goldstein, M. L. 1982, JGR, 87, 6011
Matthaeus, W. H., & Goldstein, M. L. 1986, PhRvL, 57, 495
Matthaeus, W. H., Smith, C. W., & Oughton, S. 1998, JGR, 103, 6495
Matthaeus, W. H., & Velli, M. 2011, SSRv, 160, 145
Matthaeus, W. H., Wan, M., Servidio, S., et al. 2015, RSPTA, 373, 20140154
Matthaeus, W. H., Weygand, J. M., & Dasso, S. 2016, PhRvL, 116, 245101
Mega, M. S., Allegrini, P., Grigolini, P., et al. 2003, PhRvL, 90, 188501
Monin, A. S., & Yaglom, A. M. 1971, Statistical Fluid Mechanics: Mechanics Of Turbulence (Cambridge, MA: MIT Press)
Neugebauer, M., Clay, D. R., Goldstein, B. E., Tsurutani, B. T., & Zwickl, R. D. 1984, JGR, 89, 5395
Neugebauer, M., & Giacalone, J. 2010, in AIP Conf. Proc. 1216, 12th SOLAR WIND Conf., ed. M. Maksimovic et al. (Melville, NY: AIP), 194
Neugebauer, M., & Giacalone, J. 2015, JGRA, 120, 8281
Newman, M. E. J. 2005, ConPh, 46, 323
Oboukhov, A. M. 1962, JFM, 13, 77
Osman, K. T., Matthaeus, W. H., Gosling, J. T., et al. 2014, PhRvL, 112, 215002
Osman, K. T., Matthaeus, W. H., Greco, A., & Servidio, S. 2011, ApJL, 727, L11
Osman, K. T., Matthaeus, W. H., Wan, M., & Rappazzo, A. F. 2012, PhRvL, 108, 261102
Parashar, T. N., Goldstein, M. L., Maruca, B. A., et al. 2020, ApJS, doi:10.3847/1538-4365/ab64e6
Parashar, T. N., & Matthaeus, W. H. 2016, ApJ, 832, 57
Pecora, F., Greco, A., Hu, Q., et al. 2019, ApJL, 881, L11
Politano, H., & Pouquet, A. 1998, PhRvE, 57, R21
Pollock, C. J., Burch, J. L., Chasapis, A., et al. 2018, JASTP, 177, 84
Pope, S. B. 2000, Turbulent Flows (Cambridge: Cambridge University Press)
Qudsi, R. A., Maruca, B. A., Matthaeus, W. H., et al. 2020, ApJS, doi:10.3847/1538-4365/ab5c19
Ruffolo, D., Matthaeus, W. H., & Chuychai, P. 2003, ApJL, 597, L169
Ruiz, M. E., Dasso, S., Matthaeus, W. H., & Weygand, J. M. 2014, SoPh, 289, 3917
Servidio, S., Greco, A., Matthaeus, W. H., Osman, K. T., & Dmitruk, P. 2011, JGRA, 116, A09102
Servidio, S., Valentini, F., Perrone, D., et al. 2015, JPlPh, 81, 325810107
Smith, C. W., Matthaeus, W. H., Zank, G. P., et al. 2001, JGR, 106, 8253
Smith, H. J. S. 1874, Proc. London Math. Soc., s1-6, 140
Sorriso-Valvo, L., Carbone, V., Veltri, P., Consolini, G., & Bruno, R. 1999, GeoRL, 26, 1801
Sreenivasan, K. R. 1999, RvMPS, 71, S383
Sreenivasan, K. R., & Antonia, R. A. 1997, AnRFM, 29, 435
Taylor, G. I. 1938, RSPSA, 164, 476
Tessein, J. A., Matthaeus, W. H., Wan, M., et al. 2013, ApJL, 776, L8
Tessein, J. A., Ruffolo, D., Matthaeus, W. H., et al. 2015, ApJ, 812, 68
Tessein, J. A., Ruffolo, D., Matthaeus, W. H., & Wan, M. 2016, GeoRL, 43, 3620
Tooprakai, P., Seripienlert, A., Ruffolo, D., Chuychai, P., & Matthaeus, W. H. 2016, ApJ, 831, 195
Tsurutani, B. T., & Smith, E. J. 1979, JGR, 84, 2773
Tu, C.-Y., & Marsch, E. 1995, SSRv, 73, 1
Veltri, P., & Mangeney, A. 1999, in AIP Conf. Ser. 471, SOLAR WIND 9, ed. S. T. Suess, G. A. Gary, & S. F. Nerney (Melville, NY: AIP), 543
Yordanova, E., Vaivads, A., André, M., Buchert, S. C., & Vörös, Z. 2008, PhRvL, 100, 205003
Zank, G. P., Adhikari, L., Hunana, P., et al. 2017, ApJ, 835, 147
Zank, G. P., le Roux, J. A., Webb, G. M., Dosch, A., & Khabarova, O. 2014, ApJ, 797, 28
Zhdankin, V., Boldyrev, S., Mason, J., & Perez, J. C. 2012, PhRvL, 108, 175004
Zheng, J., & Hu, Q. 2018, ApJL, 852, L23